Nanoscale Advances

ROYAL SOCIETY OF CHEMISTRY

PAPER

View Article Online
View Journal | View Issue

Cite this: *Nanoscale Adv.*, 2025, **7**, 6901

Synthesis, characterization and *in vitro* evaluation of ticagrelor and its nano-formulation targeting the NLRP3 inflammasome pathway in synovial cells

Zainab Najam, [a] Anum Gul, *[a] Muhammad Kawish, [b] Muhammad Raza Shah, [b] Tooba Aslam [a] and Nida Dastagir [a]

This *in vitro* study explored the potential of ticagrelor (TCG) and its nano-formulation, TCG-β-CD/Lec (ticagrelor-loaded beta-cyclodextrin-lecithin nano-formulation), to modulate NLRP3 inflammasome activity using the SW982 synovial cell line as a rheumatoid arthritis experimental model. TCG was entrapped in β-CD/Lec NPs *via* solvent diffusion and characterized for size, polydispersity index (PDI), zeta potential, Fourier transform infrared (FTIR) spectroscopy, and UV-Vis spectrophotometry. The average sizes of blank and TCG-loaded nanoparticles were 87.73 nm and 143.1 nm, respectively, with low PDI values (0.36 and 0.32) and zeta potentials of −6.08 and −8.69 mV, indicating stable colloidal properties. FTIR confirmed successful drug encapsulation. The synthesized NPs showed an entrapment efficiency of 57.2% and a drug loading of 43.83%. Cellular assays were conducted to assess viability (MTT), oxidative stress (H_2DCFDA and SOD activity), and the inflammatory response in the treatment groups. Gene expression of NLRP3, ASC, CASP1, and NFκB was evaluated by qRT-PCR, and IL-1β secretion was measured *via* ELISA. Compared to free TCG, the nano-formulation exhibited reduced cytotoxicity. Both TCG and TCG-β-CD/Lec significantly reduced LPS and TNF-α-induced oxidative stress, evidenced by decreased ROS levels and enhanced SOD activity. In addition, both treatment groups suppressed IL-1β secretion and downregulated key genes involved in inflammasome activation. While the nano-formulation showed comparatively better outcomes, both treatment groups demonstrated potential antioxidant and anti-inflammatory effects. Overall, the findings suggest that TCG and the TCG-β-CD/Lec nano-formulation may help regulate inflammatory responses linked to NLRP3 inflammasome activation in rheumatoid arthritis, warranting further investigation for therapeutic development.

Received 17th May 2025
Accepted 7th August 2025

DOI: 10.1039/d5na00489f

rsc.li/nanoscale-advances

1 Introduction

Rheumatoid arthritis is predominantly a systemic and progressive autoimmune condition of unknown etiology, characterized by inflammatory arthritis and extra-articular manifestations.[1] According to the Global Burden of Diseases (GBD) 2021 study, an estimated 17.6 million individuals were living with RA, globally, which is projected to hit 31.7 million by the year 2050. In South Asia, an estimated 32.5 million people had RA.[2] To date, the etiology of this disease is still not fully comprehended. However, multiple host-related and environmental risk factors have been implicated in disease progression.[3,4] The pathology of RA is characterized as heterogeneous. The common events which modulate the severity of RA involve production of autoantibodies such as rheumatoid factor (RF) and ACPAs, immune cells infiltration, dysregulated inflammation in the synovium and the expression of pro-inflammatory cytokines (such as IL-1, IL-2, TNF-α, *etc.*).[5] All these factors mediate the inflammatory process and trigger the activation of synoviocytes due to which the healthy lining structures in the synovium are converted into a pannus-like structure which invades and promotes cartilage and joint damage leading to joint deformities as well as extra-articular comorbid conditions over time.[6]

RA poses a substantial economic burden on patients and the healthcare system. Currently, the disease is not curable. However, multiple therapeutic options are available to manage disease associated symptoms and progression, thereby improving the individual's quality of life. Despite the availability of effective treatment strategies, new and better therapeutic options are still needed to manage the associated side effects and therapeutic cost and to address different response patterns of patients.[7] The recent understanding of the role of the NOD-like receptor protein 3 (NLRP3) inflammasome pathway in the regulation of inflammatory response has directed studies to investigate different inflammasome

[a]*Dow College of Biotechnology, Dow University of Health Sciences, Karachi, 75270, Pakistan. E-mail: anum.gul@duhs.edu.pk*

[b]*International Center for Chemical and Biological Sciences, H.E.J. Research Institute of Chemistry, University of Karachi, Karachi, 75270, Pakistan*

inhibitors for their efficacy against RA pathogenesis.[8] The NLRP3 inflammasome is a multimeric protein complex composed of NLRP3, ASC (apoptosis associated speck-like-protein containing a CARD) and caspase-1. The activation of NLRP3 promotes the formation of an inflammasome complex and regulates caspase 1 mediated release of proinflammatory cytokines.[9] Targeting this pathway, several drugs and natural compounds have revealed their potential as anti-inflammatory agents in various experimental studies.[10] Some potent NLRP3 inhibitors identified to date are MCC950, tranilast, CY-09 *etc.* However, these inhibitors are mostly under preclinical or clinical trial investigations and none of them have been approved for clinical application in RA yet.[11]

Ticagrelor (TCG) is an FDA approved direct acting $P2Y_{12}$ receptor antagonist. It is an ADP derivative, having rapid onset of action, high potency, and reduced response variability. The drug reversibly binds to the receptor and inhibits ADP-induced platelet aggregation thereby preventing blood clot formation.[12–14] In recent years, many studies have identified other pharmacological activities of ticagrelor besides its characteristic antiplatelet effect. Recently, a group of researchers identified that TCG has a novel pharmacological function of suppressing the NLRP3 inflammasome activity, independent of its classic $P2Y_{12}$ antagonism. The comparative analysis reported that this inhibitory response of TCG was comparable to those of other known NLRP3 inhibitors including MCC950 and CY-09.[15] In addition to this, the findings from multiple other investigations have also demonstrated that TCG can play a potential inhibitory role against NLRP3 inflammasome activation, suggesting it to be a potential therapeutic agent which can be effective in NLRP3 associated inflammatory disorders such as rheumatoid arthritis.[16–20]

According to different classification systems, TCG is categorized as a class-IV as per BCS (Biopharmaceutics Classification System) and a class-II compound as per the BDDCS (Biopharmaceutics Drug Disposition Classification System), having poor water solubility and low intestinal permeability and extensive metabolism.[21,22] The oral bioavailability of TCG is known to be ~36%.[23] To improve the bioavailability of such compounds nanodrug delivery approaches offer promising effective strategies to allow targeted delivery of pharmacological agents with enhanced efficacy and reduced off-target effects.

Cyclodextrins (CD) belong to a family of cyclic oligosaccharides made up of D-glucopyranose units. These are macrocyclic molecules having toroidal or truncated-cone-shaped structure possessing a hydrophilic exterior and hydrophobic inner cavity.[24] The amphiphilic nature allows CD molecules to encapsulate other hydrophobic molecules through host–guest interactions. Thus, the ability to form inclusion complexes is the most characteristic feature of these compounds.[25] CDs are widely used as complexing agents or as pharmaceutical excipients because of their potential ability to change the physicochemical characteristics of the guest molecules such as enhancing the stability, aqueous solubility and bioavailability, and reducing drug related toxicity and irritation.[26] The use of CDs holds "Generally recognized as safe" (GRAS) status and the regulatory status by FDA has been evolving over the years. These molecules are widely used to optimize the oral drug availability of BCS class II and IV compounds having poor water solubility.[27] Among different classes of cyclodextrins, β-CD and its derivative molecules are extensively studied for enhancing the solubility and bioavailability of hydrophobic agents. As per the 2023 CycloLab's list of CD-containing drug products available on the market, around 122 active pharmaceutical agents have been formulated using different CDs, out of which a total of 111 were reported to contain β-CD or its derivatives. This emphasized that β-CD and its derivatives are dominating the market.[28] The frequent use of β-CDs can be explained by ease of production, cheapness, ideal/optimized cavity size and complex-forming abilities with a wide range of chemicals.[29]

As NLRP3 inflammasome is considered to be a possible therapeutic target for RA, the present study was designed to evaluate the potential therapeutic role of TCG and its β-CD based nano-formulation in modulating this pathway. To date, limited research has examined the role of TCG in NLRP3-associated conditions, and, to our knowledge, none have explored its effects in an RA model. The SW982-human synovial sarcoma cell line is one of the best-known cellular models used in RA related studies. Using this cell line, the anti-inflammatory profiles of various drugs and natural compounds have been investigated.[30–34] Thus, to explore the antirheumatic effect of ticagrelor and its β-CD-conjugated nanoparticle, an *in vitro* study was conducted using the SW982 cell line as a cellular RA model. So far, based on our understanding, the role of ticagrelor in the modulation of the NLRP3 inflammasome pathway in human synovial cells has not been explored yet. As very few NLRP3 inhibitors have been available for RA, the proposed study may provide the basis for the identification of TCG and its nano-formulation as potent therapeutic agents to be used for RA after further confirmation of its effect in an *in vivo* RA model system.

2 Materials and methods

2.1 Chemicals & reagents

Dulbecco's Modified Eagle's Medium (DMEM 1×) (cat # 11965092), heat inactivated-Fetal Bovine Serum (FBS) (cat # 10500064), TryplE Select Enzyme (1×) (cat # 12563-011), Phosphate Buffered Saline (PBS 10×), and trypan blue (cat # 15250-061) were obtained from Gibco (Life Technologies Corp. USA). L-Glutamine (cat # G7513), penicillin–streptomycin (cat # P4333), LPS (L4516), soya lecithin and beta-cyclodextrin (β-CD) were acquired from Sigma-Aldrich. The MTT tetrazolium dye (cat # A600799) was obtained from BBI life sciences. 2′-7′-Dichlorofluorescein diacetate (H_2DCFDA) (cat # D399) and DAPI (4′,6-diamidino-2-phenylindole, dihydrochloride) (cat # D1306) were obtained from Invitrogen (Life Technologies Corp. USA). Ticagrelor (cat # A543807) was obtained from Ambeed, USA, and TNF-α (RPA133Hu01) was procured from Cloud Clone Corp. The purchased solvents were of HPLC grade and obtained from Fisher Scientific, UK, through a local supplier.

2.2 Synthesis of blank and TCG loaded nano-formulations

The synthesis of blank-β-CD/Lec and its drug conjugated formulation TCG-β-CD/Lec was carried out using a solvent

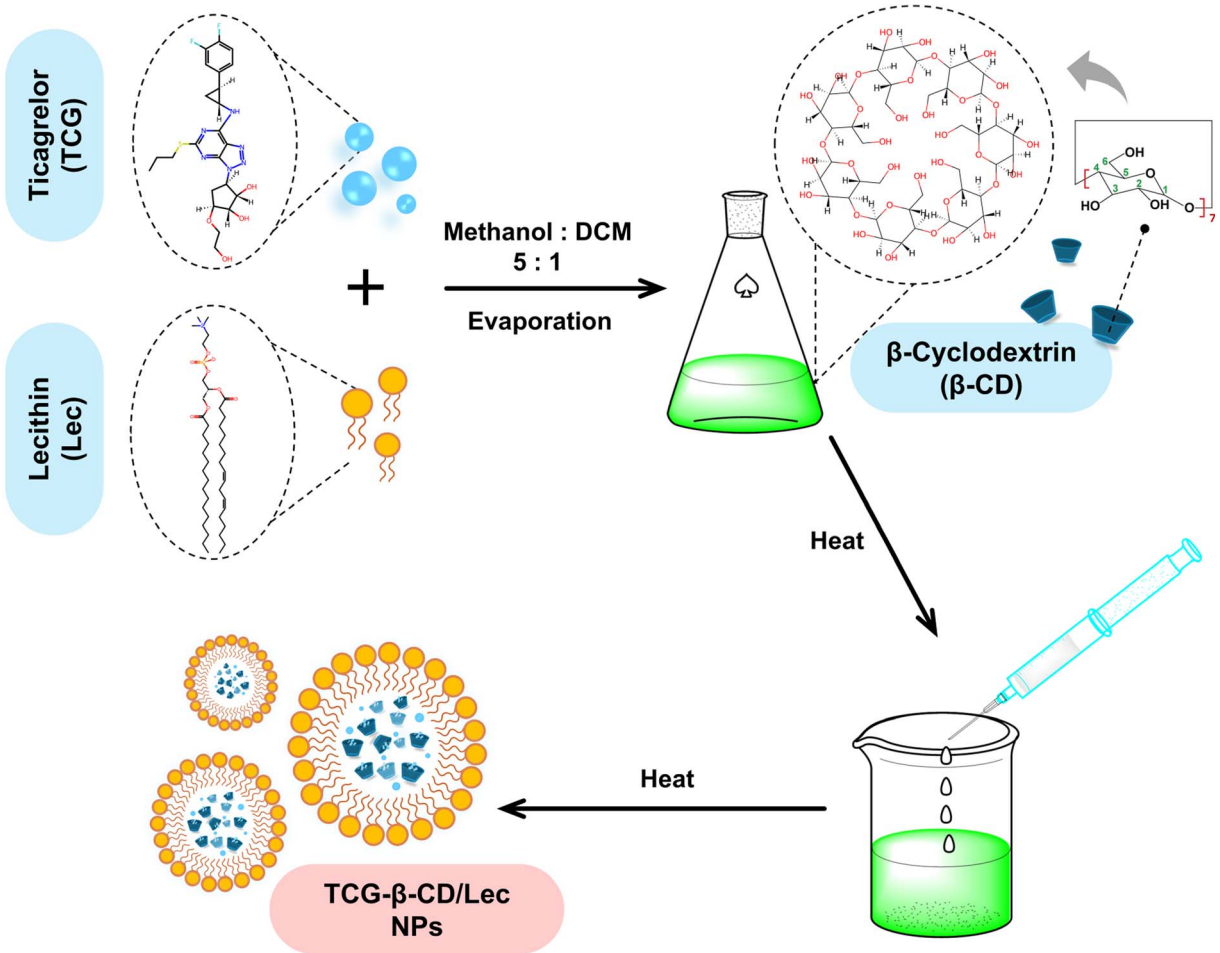

Fig. 1 Schematic representation for the preparation of TCG-β-CD/Lec NPs. All chemical structure images were adapted from ChemSpider.[35]

dispersion method (Fig. 1). Briefly, soya lecithin (20 mg) and TCG (5 mg) were dissolved in a solvent mixture containing methanol and dichloromethane (DCM) (5 : 1). The solution was then sonicated to ensure complete dissolution. Then 10 mL of DI water was added to a 50 mL beaker containing 5 mg of β-CD under constant temperature conditions (40 °C). The organic solution containing drug and lecithin was then introduced dropwise into the aqueous phase. After the complete evaporation of the organic solvent, the aqueous phase containing TCG-β-CD/Lec NPs was centrifuged at 12 000 rpm, and the supernatant was discarded. The obtained pellet was then successively washed with organic solvent to remove unbound drug and freeze dried, followed by rehydration in DI water. The homogeneity of the suspension was enhanced *via* probe sonication (VC 505/VC 750, Sonics, Newtown, USA) for 5 min and stored at 4 °C for further use. The blank-β-CD/Lec NPs were prepared with the aforementioned method except TCG additions.

2.3 Characterization of blank-β-CD/Lec and TCG-β-CD/Lec NPs

2.3.1 Hydrodynamic diameter, polydispersity index (PDI) and zeta potential analysis. The average size, PDI and zeta potential of the prepared nanoparticles were determined using a Zetasizer (Zetasizer Nano ZS90, Malvern Instruments, Malvern, UK). In brief, nanosuspensions were carefully poured into a plastic cuvette in order to minimize bubble formation. The cuvette was then placed in the instrument, and analysis was carried out at ambient temperature. The medium viscosity, pressure and refractive index were set at 1.0, 80.4 and 1.33, respectively.

2.3.2 Fourier transform infrared (FTIR) spectroscopy. FTIR spectroscopy was performed to evaluate surface functionalization and assess possible drug entrapment. For this purpose, potassium bromide (KBr) discs, composed of a mixture of dried samples (TCG, blank β-CD/Lec, and TCG-β-CD nanoformulation) and KBr, were used and the spectra was recorded in the range of 4000–400 cm^{-1} by using an FTIR spectrophotometer.

2.3.3 Drug loading and entrapment efficiency analysis. The drug loading efficiency of TCG-β-CD/Lec NPs was determined using a method adapted from protocol.[36] Briefly the nanosuspensions (2 mL) were subjected to centrifugation at a speed of 10 000 rpm for 10 min as described. The supernatant containing free drug was discarded and the pellet was dispersed in methanol and the drug was estimated at 255 nm using a UV-Vis spectrophotometer. The percentage of drug entrapment

efficiency and loading content were calculated by using the following equations:

$$\%\ \text{Drug entrapment} = \frac{\text{amount of drug used} - \text{unloaded drug}}{\text{amount of drug used}} \times 100$$

$$\%\ \text{Loading content} = \frac{\text{amount of drug in solution}}{\text{amount of drug taken for loading}} \times 100$$

2.3.4 *In vitro* release study. The release profiles of TCG in both buffer solutions of pH 7.0 and 4.0 containing 1% Tween 80 were studied employing the *in vitro* dialysis technique. Briefly, 2 mL of TCG-β-CD/Lec NPs (2.5 mg mL^{-1}) was placed in the buffers (pH 7.0 and 4.0) and was transferred to the dialysis bag after which a clamp was fixed at both ends. The dialysis bag was gently transferred to a beaker containing 40 mL of the buffer at a pH of 7.0 and 4.0, respectively. Subsamples of 2 mL were taken at predetermined time intervals, and the equivalent volume of the buffer was replaced in the flask to produce a concentration gradient. The amount of TCG released content in the solution was determined at different time intervals using a UV-Vis Spectrophotometer at lambda max of 255 nm.

2.4 Cell culture

Two human cell lines, including SW982 (HTB-93™, synovial sarcoma) and BJ (CRL-2522™, normal fibroblast), were acquired from ATCC. Both cell lines were cultured as per standard cell culture procedures in sterile growth medium DMEM-high glucose supplemented with FBS (10%) and 1% antibiotics (pen–strep) solution. All the required culture conditions had been maintained in the cell culture incubator with a humidified atmosphere at 37 °C and 5% CO_2. To conduct *in vitro* cell culture experiments, nano-formulations with and without ticagrelor, *i.e.* TCG-β-CD/Lec and blank-β-CD/Lec formulations, were diluted in DI water to achieve concentrations equivalent to TCG as per the provided characterization data.

2.5 Cell viability assay

For estimating the impact of the prepared nano-formulations on cell survival, the MTT assay was performed on two different cell lines (SW982 and BJ). For experimental purposes, cells were plated out into a 96-well culture plate and the basic assay protocol was followed with optimized conditions.[37] The seeding densities for SW982 and BJ cells were 3.5×10^3 and 10×10^3 cells per well, respectively. After seeding for 24 h, the cultured cells were subjected to treatment with different doses (within the range of 1–100 μg mL^{-1}) of TCG, TCG loaded nano-formulation (TCG-β-CD/Lec) and formulations without TCG (blank-β-CD/Lec) at an equivalent concentration of TCG and incubated for 48 h. Next, the culture medium was replaced with MTT solution (final conc. 0.5 mg mL^{-1} in fresh media). After incubating the plate for 4 h, MTT solution was carefully removed from all the wells. In the last step, the resulting formazan crystals were completely solubilized with DMSO (100 μL per well) on a plate shaker for ~5 min (in the dark) until complete solubilization. Finally, the results were obtained by measuring absorbance at 570 and 540 nm with a microplate reader (Varioskan™ LUX, Thermo Scientific™) and cell viability was analyzed using the following equation:

$$\%\ \text{Cell viability} = \left(\frac{\text{OD}_{(\text{sample})} - \text{mean OD}_{(\text{blank})}}{\text{mean OD}_{(\text{control})} - \text{mean OD}_{(\text{blank})}}\right) \times 100$$

2.6 Reactive oxygen species (ROS) analysis

For analyzing the effect of TCG and TCG-β-CD/Lec nano-formulation on intracellular ROS production, a fluorescent dye, H_2DCFDA, was used to measure ROS activity. For this assay, SW982 cells (3.5×10^3 cells per well) were cultured in a 96-well plate for 24 h. Next, the cells were pre-treated with TCG, TCG-β-CD/Lec and blank-β-CD/Lec groups at 0.1 μg mL^{-1} concentration, followed by stimulation with LPS and TNF-α (200 and 50 ng mL^{-1}, respectively), for 24 h. In this experiment, the untreated cells represent the negative control whereas treatment with H_2O_2 (500 μM, for 15 min) was used as standard control. At the end of compounds treatment, the supernatant was discarded from wells and cells were rinsed with DMEM (1×) followed by incubation with H_2DCFDA dye (10 μM) for 1 hour in an incubator. After that, the dye solution was taken out and cells were subsequently rinsed with DMEM and PBS (1×).[38] Finally, fluorescent images were captured using the green channel on a fluorescence microscope (DMi8-Leica). All images were then analyzed with ImageJ software program (version-1.54i, National Institute of Health, NIH-USA)[39] and mean fluorescence intensity was measured in all groups.

2.7 Superoxide dismutase (SOD) assay

This assay was performed to measure the activity of SOD enzyme using a Superoxide Dismutase (SOD) Colorimetric Assay Kit (cat # EIASODC, Invitrogen, USA). For sample preparation, SW982 cells (1×10^6 per mL, each well) were plated for 24 h into 6-well culture plates and then subjected to TCG and TCG-β-CD/Lec treatment at 0.1 μg mL^{-1} concentration, followed by stimulation with LPS and TNF-α (200 and 50 ng mL^{-1}, respectively). After treatment, the culture plates were incubated for 24 h. Next, the cell lysate samples were prepared, and the assay was performed following the instructions provided by the kit's manufacturer. On completion of the assay, the absorbance signal was recorded at 450 nm with a microplate reader (Varioskan™ LUX). The concentration of SOD enzyme was then determined by standard curve analysis using GraphPad Prism software.

2.8 Gene expression analysis

2.8.1 RNA extraction and quantification. For gene expression analysis RNA extraction was performed first. For this purpose, SW982 cells (1×10^6 per mL, each well) were cultured for 24 h into 6-well culture plates, followed by treatment similarly as described earlier in SOD assay. After treatment with compounds for 24 h, the RNA extraction steps were performed

with TRIzol™ Reagent (cat # 15596026, Invitrogen, USA) as per the manufacturer's protocol for cells grown in a monolayer. The extracted RNA samples from each group were analyzed for quantification and purity using a NanoDrop spectrophotometer (Thermo™). Additionally, the integrity of extracted RNA samples was confirmed by gel electrophoresis using 1% agarose gel with SYBR™ Safe DNA Gel Stain (cat # S33102, Invitrogen, USA).

2.8.2 cDNA synthesis. Next, the reverse transcription step was carried out with 1 μg of the extracted total RNA to synthesize cDNA in a thermal cycler (Bio-Rad C1000 Touch™). For this step a RevertAid First Strand cDNA Synthesis kit (cat # K1622, Thermo™) was used, following the instructions provided with the kit. The synthesized cDNA samples were then stored at −80 °C until further use.

2.8.3 Primer designing. For primer designing, the National Center for Biotechnology Information (NCBI) program was accessed to retrieve the sequences of NLRP3 inflammasome related genes through the reference sequence (RefSeq) database. Primers for all target genes were designed using Primer3web (version 4.1.0) and then subjected to the NCBI-BLAST tool as well as the OligoCalc online tool for oligonucleotide properties calculation to assess primer specificity.[40,41] All primers were then reconstituted in nuclease free water and stored as specified by the manufacturer. The sequences of all gene specific primers are listed in Table 1.

2.8.4 RT-PCR. Quantitative real time PCR (qRT-PCR) analysis was carried out to estimate the gene expression level of NLRP3, ASC, CASP-1, and NFκB genes by using Maxima SYBR Green/ROX qPCR Master Mix (cat # K0221, Thermo™). Using a QuantStudio™ 7 Flex RT-PCR System (Applied Biosystems), all the experiments were run under specified thermal conditions as mentioned in Table 2, and the reaction was completed with melt curve analysis at the end. Finally, the comparative C_T analysis method ($2^{-\Delta\Delta C_T}$) was applied for relative mRNA quantification in all samples.

2.9 Enzyme linked immunosorbent assay (ELISA)

The anti-inflammatory effect of TCG and its nano-formulation was evaluated by measuring the interleukin-1β (IL-1β) level using ELISA. Cell seeding was performed and treatment conditions were evaluated as described for the SOD assay. Next, the cell culture supernatants were collected and processed following the instructions in the IL-1β ELISA kit manual (SEA563Hu, Cloud-Clone Corp.) The assay was performed in accordance with the provided manufacturer's protocol, and absorbance was measured at 450 nm using a microplate reader (Varioskan™ LUX). The concentration of inflammatory cytokine IL-1β was then determined by standard curve analysis using GraphPad Prism software.

Table 2 Steps for qRT-PCR reaction

Step	Temperature (°C)	Time	No. of cycles
Initial denaturation	95	2 min	1
Denaturation	95	15 s	40
Annealing	60	30 s	
Extension	72	30 s	

2.10 Statistical analysis

The graphical representation of all the results and standard curve analysis were performed with GraphPad-Prism software (version-10). The resulting data values in this study were reported as mean ± standard error of the mean (SEM) from three biological replicates measured in triplicate ($n = 3$). The data was statistically analyzed with SPSS Statistics program (version release-26.0, IBM Corp.). For group comparisons, one-way ANOVA and subsequent *post hoc* analysis (based on the normality and homogeneity of variance tests) was done. Statistical significance was determined by a p-value of 0.05 or lower ($p \leq 0.05$).

3 Results and discussion

3.1 Hydrodynamic diameter, PDI, and zeta potential analysis

The average sizes of blank-β-CD/Lec and TCG-β-CD/Lec NPs were found to be 87.73 ± 43.3 nm and 143.1 ± 13.6 nm. Increment in size was observed in case of TCG-β-CD/Lec NPs which may be due to the inclusion of TCG within the interior hydrophobic environments of β-CD/Lec NPs suggesting its potential for biomedical applications.[42] The polydispersity index suggests the colloidal homogeneity of the nanosuspension, and the value greater than 0.5 indicates the size broadening of the nanosuspension. The PDI values of both blank-β-CD/Lec and TCG-β-CD/Lec NPs were 0.36 ± 0.04 and 0.32 ± 0.08, respectively, signifying the colloidal homogeneity of the developed nanoparticles. Zeta potential analysis measures the potential difference between two distinct phases and the higher values represent colloidal stability. The zeta potential values of blank-β-CD/Lec and TCG-β-CD/Lec NPs were −6.08 ± 0.47 mV and −8.69 ± 0.68 mV, respectively. The increased zeta potential values in case of TCG-β-CD/Lec NPs reflect that the drug entrapment within hydrophobic cavities and the liposomes increases the colloidal stability of TCG-β-CD/

Table 1 Sequences of Primers

Gene	Accession no.	Forward (5′–3′)	Reverse (5′–3′)	Product size
GAPDH	NM_002046	TTGGTCGTATTGGGCGCCTG	TCCCGTTCTCAGCCTTGACG	165
NLRP3	NM_001243133	AGAGCCCCGTGAGTCCCATT	TTTTCCCAATCCCTGCCGCC	108
ASC	NM_013258	CGCCGAGGAGCTCAAGAAGT	GTGAGGTCCAAGGCGTCCAT	111
CASP1	NM_001257118	CCAGATGGTAGAGCGCAGATG	TCCCACACTCCCGACCATACA	138
NFκB	NM_021975	AAGGAACGCTGTCAGAGGCC	GTTGTCGACGGATGCCAGGT	116

Lec NPs.[42] Nanoparticle-mediated delivery systems are increasingly being employed for targeted and site-specific administration of drugs. It has been reported that NPs with diameter below 500 nm can effectively permeate the biological barriers thereby maximizing the therapeutic index of the drug.[43]

3.2 FTIR analysis of the synthesized nano-formulations

Lecithin (Lec) is widely used in food industries to regulate the lipid profile in the body. When tested at 20 g daily it has been established to be safe and compatible with the human body. Lec is an amphiphilic molecule that belongs to the classes of phospholipids and which self-assemble in an aqueous environment.[44] This biocompatibility and amphiphilicity make it an attractive drug delivery agent for delivering various drug molecules. The association of beta-cyclodextrin (β-CD) with Lec not only enhances the prolonged circulation but has the ability to entrap the hydrophobic drug within its interior cavity. In this study, TCG, a hydrophobic drug was entrapped in lecithin NPs *via* solvent diffusion method (Fig. 1) followed by freeze drying and the reconstitution in DI water, enhances the colloidal stability of TCG-β-CD/Lec NPs. The stacking of TCG and β-CD/Lec NPs was characterized by FTIR spectroscopy. Blank-β-CD/Lec NPs showed characteristic frequencies of OH, C=O, C–H and C–O stretching at 3331 cm^{-1}, 1745 cm^{-1}, 2940 cm^{-1}, and 1020 cm^{-1}. The FTIR spectra of TCG show characteristic absorption around 1623 cm^{-1} and 1513 cm^{-1} corresponding to N–H stretching.[45] The C–H, C–OH and C–O stretching vibrations were also observed around 2945 cm^{-1}, 1210 cm^{-1}, and 1042 cm^{-1}. The stretching frequencies at 3390 cm^{-1} and 3292 cm^{-1} correspond to OH and NH_2 stretching, respectively (Fig. 2). The FTIR spectra of TCG-β-CD/Lec NPs show very slight variations in drug frequencies which suggests that TCG is chemically stable within TCG-β-CD/Lec NPs.[46,47]

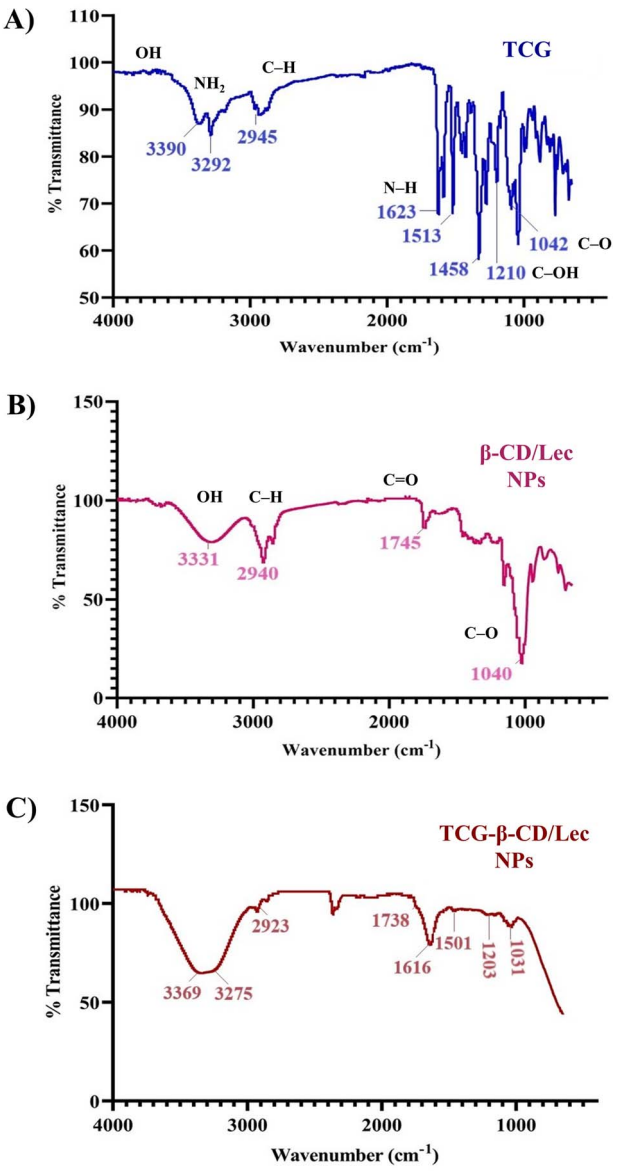

Fig. 2 FTIR spectral analysis. FTIR spectra of (A) TCG, (B) β-CD/Lec NPs, and (C) TCG-β-CD/Lec NPs, showing characteristic functional groups.

3.3 Drug loading and entrapment efficiency

The chemical characteristic of the drug and its interaction with the carrier molecules influenced the effectiveness of drug entrapment and its controlled release.[48] There is a need for increased drug loading efficiency to ensure that the drugs that are to be delivered to the target site are delivered in larger concentrations to achieve higher therapeutic effects. Moreover, increased drug loading also contributed to improved sustainability of the nano-formulation.[49] The drug entrapment efficiency and loading content of TCG-β-CD/Lec NPs was found to be 57.2 ± 1.23%, whereas the loading content was found to be 43.83 ± 1.12%. The higher drug loading can be attributed to the lipophilicity of both TCG and Lec molecules.[49] Moreover, the presence of β-CD molecules can also promote drug entrapment through increased molecular interaction.

3.4 *In vitro* release study

For any drug delivery approach, the drug release kinetics is one of the important parameters which allows the assessment of prepared nano-formulations at different pH. The *in vitro* drug release profiles of TCG showed that the prepared TCG-β-CD/Lec nano-formulation gives a higher release of 67.1 ± 0.36% at pH

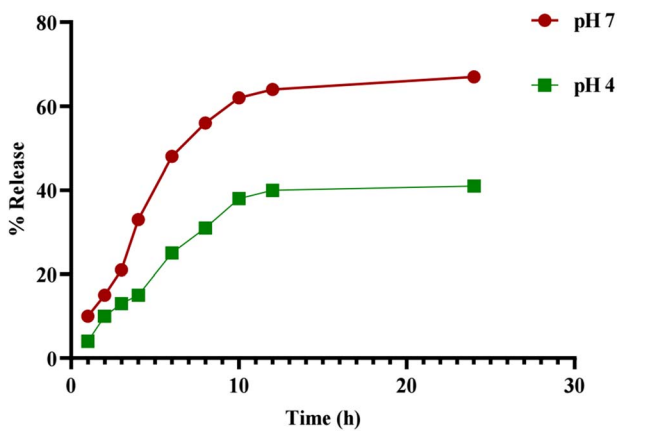

Fig. 3 *In vitro* release profiles of TCG release at different pH.

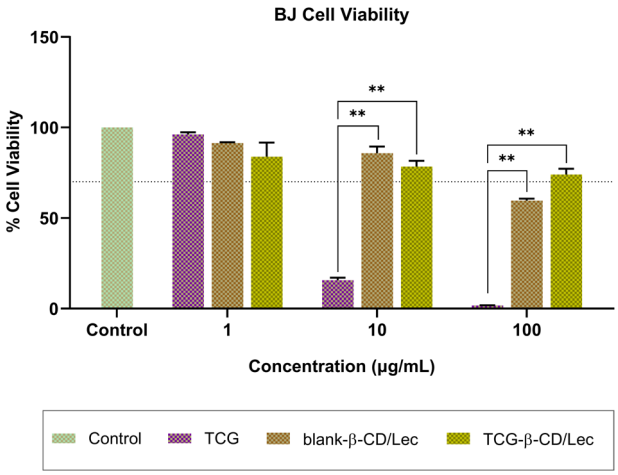

Fig. 4 Effect of TCG and TCG-loaded nano-formulation on BJ cell viability. Graphical representation of % cell viability of TCG, TCG-β-CD/Lec and blank-β-CD/Lec formulations at different concentrations (1–100 µg mL^{-1}) against the BJ cell line. Data is presented as mean ± SEM ($n = 3$). One-way ANOVA followed by Games–Howell's *post hoc* test was applied for multiple comparisons (**$p \leq 0.01$).

7.0, after 12 h, in contrast to 41.4 ± 0.63% at pH 4.0, as depicted in Fig. 3. Previous findings indicate that the amine and hydroxyl groups are key contributors for higher stacking of drugs.[50] In this study the secondary interaction in the form of β-CD molecules and their hydrophobic cavity along with lipophilicity of lecithin may have resulted in the entrapment of TCG in higher amount providing sustained release at pH 7 against time.

3.5 Cell viability assay

The *in vitro* cytotoxic effects of TCG, blank-β-CD/Lec and TCG-β-CD/Lec formulations were analyzed against BJ and SW982 cells, subjected to treatment for 48 h. The results were inferred as per the standard limits, defined by the International Organization for Standardization (ISO), "the decrease in cell viability by >30% (*i.e.*, viability less than 70%) is considered potential cytotoxic effect".[51]

In BJ cells, the treatment with TCG showed a nontoxic effect (96.1% cell viability) at 1 µg mL^{-1} concentration, whereas concentrations above 1 µg mL^{-1} TCG showed a significant cytotoxic effect. In contrast to this, the TCG-β-CD/Lec nano-formulation showed non-cytotoxic effects up to 100 µg mL^{-1} concentration with >73% cell viability, as compared to TCG which showed significant toxicity at 100 µg mL^{-1} concentration with only 1.7% cell viability ($p \leq 0.01$). Additionally, the blank-β-CD/Lec group showed >85% cell viability up to 10 µg mL^{-1} tested concentration in BJ cells (Fig. 4 and 5). In SW982 cells, TCG showed non-cytotoxic effects up to 12.5 µg mL^{-1} concentration with >85% cell viability, whereas for the TCG-β-CD/Lec

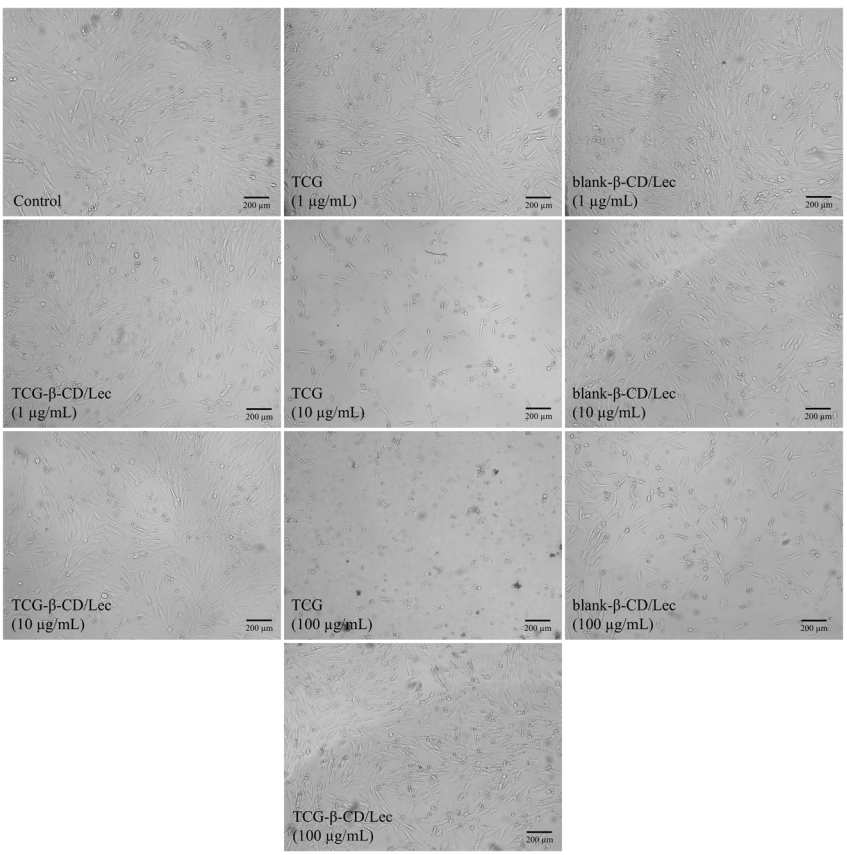

Fig. 5 Morphological observation of BJ cell viability against TCG and its nano-formulation treatment. Representative microscope images showing the effect of TCG, TCG-β-CD/Lec and blank-β-CD/Lec formulations on the viability of BJ cells at different concentrations (1–100 µg mL^{-1}). All images were captured at 100× magnification using an inverted microscope (Leica DMi1).

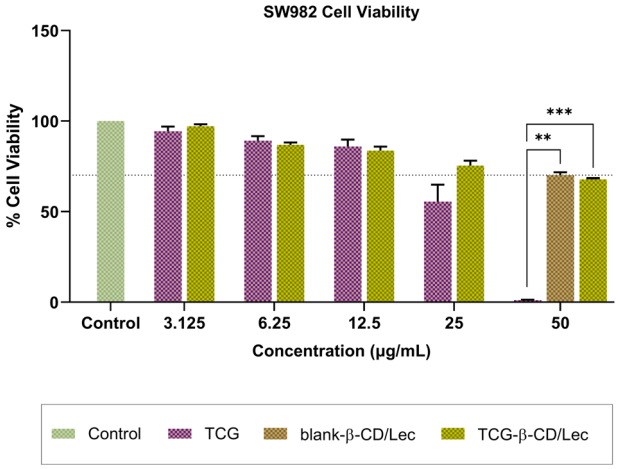

Fig. 6 Effect of TCG and the TCG-loaded nano-formulation on SW982 cell viability. Graphical representation of % cell viability of TCG, TCG-β-CD/Lec and blank-β-CD/Lec formulations at different concentrations (3.125–50 µg mL^{-1}) against the SW982 cell line. Data is presented as mean ± SEM (n = 3). One-way ANOVA followed by Games–Howell's *post hoc* test was applied for multiple comparisons (**$p \leq 0.01$, ***$p \leq 0.001$).

nano-formulation, the non-cytotoxic effect was found up to 25 µg mL^{-1} conc. with >75% viability, compared to the treatment with 25 µg mL^{-1} TCG for which 55.5% cell viability (*i.e.*, cytotoxic effect) was observed. Moreover, the treatment with the blank-β-CD/Lec group showed 70.6% cell viability at 50 µg mL^{-1} in SW982 cells as shown in Fig. 6 and 7. The resulting data is supported by multiple studies where TCG showed no significant cytotoxicity at concentrations up to 12.5 µg mL^{-1}, among different cell lines.[52–54] Furthermore, the results obtained for TCG-β-CD/Lec groups showed that the nano-formulation treatment notably decreased TCG associated toxicity at higher concentrations. Based on the cytotoxicity profiling, the concentration 0.1 µg mL^{-1} of each group was selected for further experiments.

3.6 Reactive oxygen species (ROS) analysis

As a measure of cellular oxidative stress, the level of ROS production was observed in response to different treatment groups. The H_2O_2 treated cells served as a reference control to compare the level of ROS production in LPS and TNF-α stimulated cells. Fig. 8(A) shows the representative fluorescence microscopic images of LPS and TNF-α induced ROS production in different treatment groups. The results from the analysis showed that ROS production was significantly induced ($p \leq 0.001$) in response to both LPS and TNF-α induction compared to normal untreated cells and the effect in both groups was comparable with that of the H_2O_2 treated control. When compared to the LPS-induced control, the level of ROS

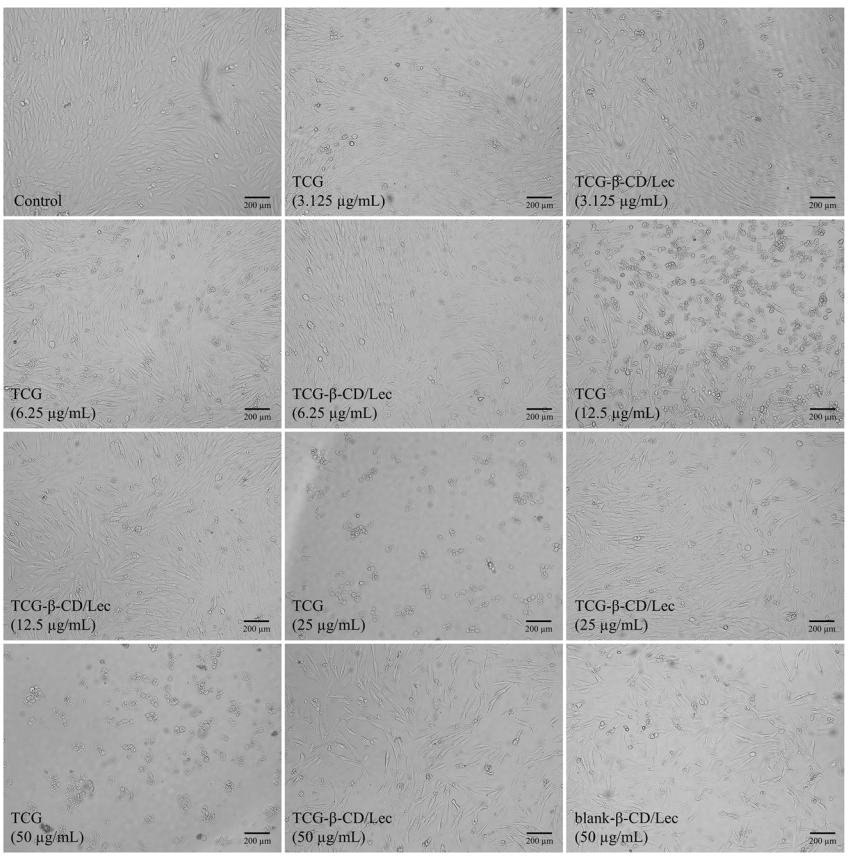

Fig. 7 Morphological observation of SW982 cell viability against TCG and its nano-formulation treatment. Representative microscope images showing the effect of TCG, TCG-β-CD/Lec and blank-β-CD/Lec formulations on the viability of SW982 cells at different concentrations (3.125–50 µg mL^{-1}). All images were captured at 100× magnification using an inverted microscope (Leica DMi1).

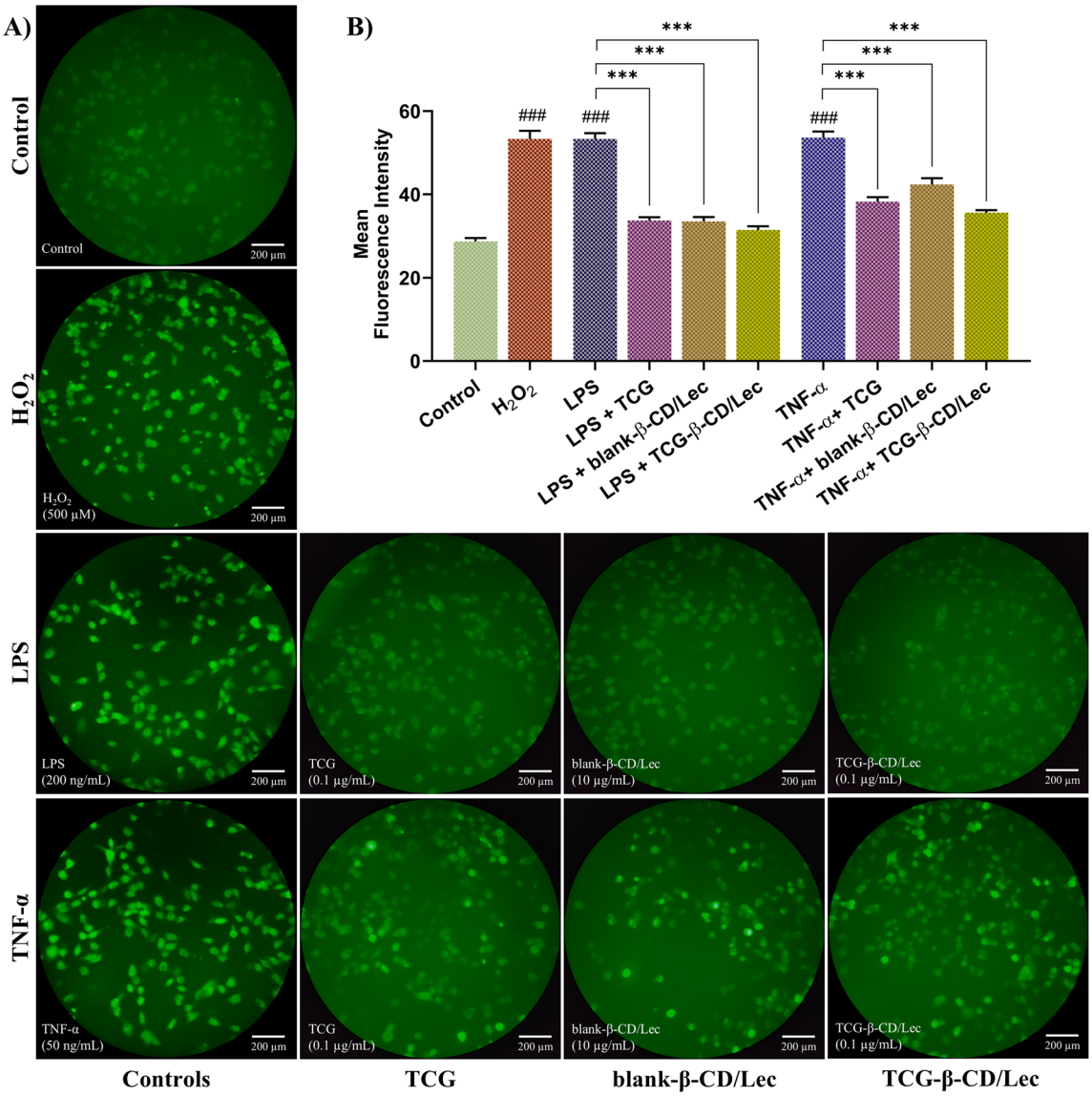

Fig. 8 Effect of TCG and its nano-formulation on oxidative stress. (A) Representative fluorescence microscopy images of ROS production in LPS and TNF-α stimulated SW982 cells pretreated with TCG, TCG-β-CD/Lec or blank-β-CD/Lec nano-formulation. All images captured at 200× magnification. (B) Quantification of mean fluorescence intensity indicating significant reduction in ROS levels across all treatment groups. Data is presented as mean ± SEM ($n = 3$). For multiple comparison analysis, Games–Howell's *post hoc* test was used. $^{###}p \leq 0.001$ *vs.* untreated control and $^{***}p \leq 0.001$ *vs.* respective inducer controls (LPS or TNF-α).

production was substantially decreased in all treatment groups having a significant difference of $p \leq 0.001$. The inhibition of LPS-induced ROS production by the treatment groups was evident from the decrease in green fluorescence intensity. Relative to the TNF-α induced control, the treatment with all the investigated compounds significantly decreased the level of ROS production with $p \leq 0.001$, as observed in LPS-stimulated cells. The resulting data indicate the better inhibitory effect of the TCG nano-formulation on ROS production compared to that of free TCG as observed with fluorescence microscopy analysis (Fig. 8).

Studies conducted on different disease models showed that TCG treatment decreases the aberrant ROS production that may contribute to restoring normal functions. The study conducted on the angiotensin II-induced endothelial dysfunction model in rat showed that TCG administration significantly reduced the ROS production in the aorta obtained from *ex vivo* culture.[55] Two other studies were conducted to explore the cardioprotective effect of TCG using the H9c2 cardiomyocyte cell line as cellular models mimicking insulin resistance and diabetic cardiomyopathy. The results from both studies showed that TCG treatment markedly decreased the cellular ROS generation in insulin-resistant and hyperglycemic (HG) cardiomyocytes.[56,57] Consistent with the results in the literature, the present study observed a decrease in ROS production for TCG and its nano-formulation treatment in LPS and TNF-α stimulated SW982 cells compared to the control groups.

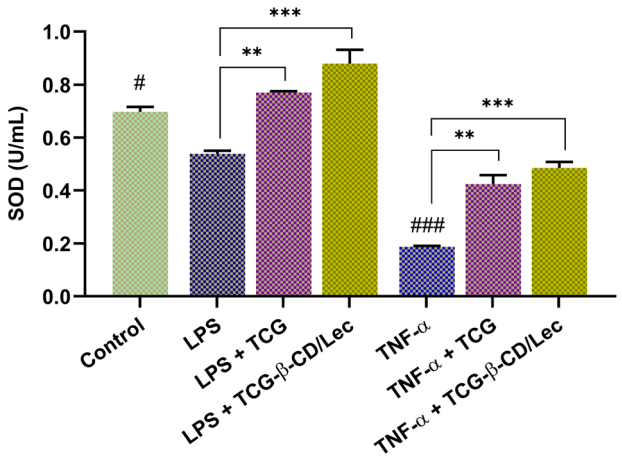

Fig. 9 Effect of TCG and the TCG-loaded nano-formulation on antioxidant enzyme activity. Graphical representation of the SOD level in LPS and TNF-α induced SW982 cells treated with TCG or TCG-β-CD/Lec nano-formulation. Data is presented as mean ± SEM ($n = 3$). For multiple comparison analysis, Tukey's *post hoc* test was used. Symbol # indicates a significant reduction in the enzyme level of LPS and TNF-α treated controls relative to the untreated control cells ($^{\#}p \leq 0.05$, $^{\#\#\#}p \leq 0.001$). Symbol * indicates a significant increase in SOD activity of the respective treatment groups compared to the LPS or TNF-α control groups ($^{**}p \leq 0.01$, $^{***}p \leq 0.001$).

3.7 Superoxide dismutase (SOD) activity analysis

In the LPS and TNF-α stimulated cells which were pretreated with TCG and the TCG-loaded nano-formulation, the antioxidant activity of SOD enzyme was analyzed. The resulting data indicated that the SOD levels in LPS and TNF-α treated control groups were significantly reduced compared to those of the untreated group (normal control cells) with $p \leq 0.05$ and $p \leq 0.001$, respectively.

When compared to the LPS-stimulated control cells, significantly enhanced SOD activity was found in response to TCG treatment with $p \leq 0.01$. Relative to this, TCG-β-CD/Lec also showed increased production of SOD enzyme with $p \leq 0.001$, representing the better activity of the TCG-nano-formulation compared to free TCG (Fig. 9). With respect to the TNF-α stimulated control group, the treatment with TCG showed significantly higher SOD levels with $p \leq 0.01$. In contrast to this, the TCG-β-CD/Lec nano-formulation showed statistically better activity and exhibited increased production of SOD activity with $p \leq 0.001$, as shown in Fig. 9.

The findings from ROS and SOD assay suggest that TCG and its nano-formulation may contribute to the alleviation of oxidative stress by suppressing ROS production and restoring SOD activity in synovial cells, as observed in this study. To the best of our knowledge, no prior studies have assessed the effects of TCG on ROS and SOD levels in the context of RA pathophysiology. Therefore, this work may represent one of the first investigations exploring the antioxidant potential of TCG and its nano-formulation in an RA model.

3.8 Gene expression analysis

In this experiment, the untreated cells served as the normal control group, whereas cells stimulated with LPS and TNF-α served as the positive control. The expression level of all study genes was subjected to normalization against the GAPDH level, serving as a reference gene. Fig. 10(A) represents the effect of different treatment groups on LPS-triggered expression of NLRP3 inflammasome associated genes. In comparison with the untreated control cells, the LPS-induced control groups showed significant upregulation in the levels of NLRP3, CASP1, and NFκB with $p \leq 0.001$, whereas for the ASC gene, a non-significant increase in the expression was found. Relative to the LPS-induced control cells, the treatment with TCG showed a non-significant decrease in NLRP3, ASC and CASP1 expression, whereas significant downregulation of NFκB levels was observed in response to TCG, with $p \leq 0.001$. In contrast to this, the treatment with the TCG-β-CD/Lec nano-formulation exhibited significant downregulation of CASP1 and NFκB levels with $p \leq 0.05$, whereas a non-significant decrease in NLRP3 expression was observed.

Fig. 10(B) displays the effect of different treatment groups on TNF-α induced expression of NLRP3 inflammasome associated genes. The mRNA levels of all four genes (NLRP3, CASP1, and NFκB and ASC) were strongly induced as a result of TNF-α stimulation with a significant difference of $p \leq 0.001$ compared to normal control cells. Relative to the TNF-α control

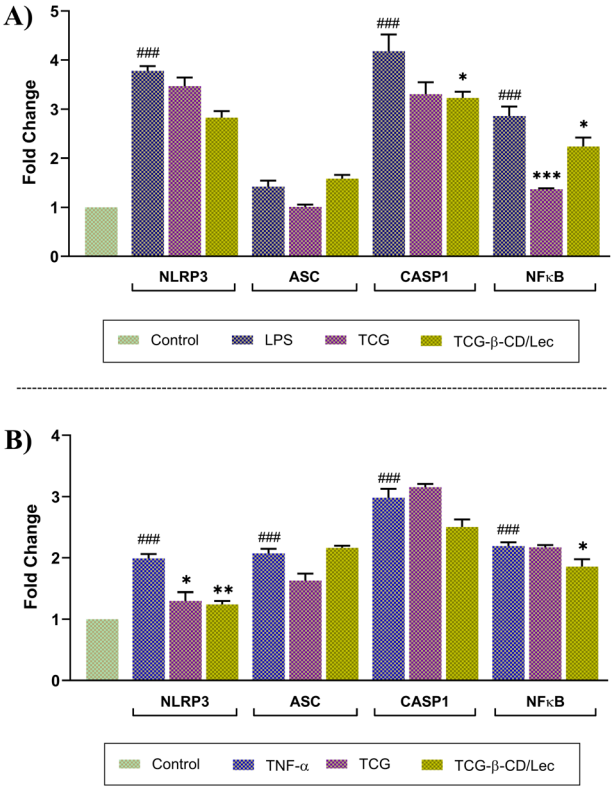

Fig. 10 Effect of TCG and its nano-formulation on the expression of NLRP3 inflammasome related genes. The graph represents the mean fold change in the mRNA expression of NLRP3, ASC, CASP1, and NFκB genes in (A) LPS and (B) TNF-α induced cells treated with TCG and TCG-β-CD/Lec groups. Data is shown as mean ± SEM ($n = 3$). For multiple comparison analysis, Tukey's *post hoc* test was applied. $^{###}p \leq 0.001$ *vs.* untreated control; $^{*}p \leq 0.05$, $^{**}p \leq 0.01$, $^{***}p \leq 0.001$ *vs.* respective inducer controls (LPS or TNF-α).

cells, the treatment with TCG and TCG-β-CD/Lec groups resulted in a significant reduction of NLRP3 expression with $p \leq 0.05$ and $p \leq 0.01$, respectively. However, for the ASC gene, no significant effect of TCG and TCG-β-CD/Lec treatments was found on the mRNA expression level. Additionally, for the expression of CASP1 gene, non-significant effect was observed for all treatment groups. Moreover, for the NFκB gene, no significant effect was found for TCG treatment, whereas treatment with TCG-β-CD/Lec showed significant reduction in NFκB expression with $p \leq 0.05$.

In line with the present study, previous research has also shown the inhibitory action of TCG on NLRP3 inflammasome associated genes. The study performed using the ischemia–reperfusion model of type 2 diabetic rats showed that TCG attenuates post reperfusion up-regulated expression of CASP1, IL-1β, NLRP3, and ASC.[20] In the type 2 diabetes mouse model of itching, the treatment with TCG was found to reduce the up-regulation of NLRP3 and CASP1 (at both transcriptional and protein levels) and ASC (at the protein level).[58] Moreover, it was also established that NFκB positively regulates NLRP3 expression in macrophages through the RelA/miR-30a/NLRP3 signaling axis of NLRP3 inflammasome pathway in RA. Thus, targeting this pathway new treatment targets can be explored for RA treatment.

3.9 Enzyme linked immunosorbent assay (ELISA)

The effect of TCG and its nano-formulation on inflammatory cytokine production was assessed by measuring the levels of IL-1β through ELISA. IL-1β production was strongly induced in response to both the LPS and TNF-α stimulation compared to the normal (untreated) group, showing statistically significant increases ($p \leq 0.01$ and $p \leq 0.05$, respectively). In contrast, pre-treatment with both TCG and TCG-β-CD/Lec significantly reduced IL-1β levels relative to the LPS-stimulated group ($p \leq 0.01$). A comparable reduction was observed in TNF-α stimulated cells, with both treatments resulting in significantly lower IL-1β levels ($p \leq 0.05$) (see Fig. 11).

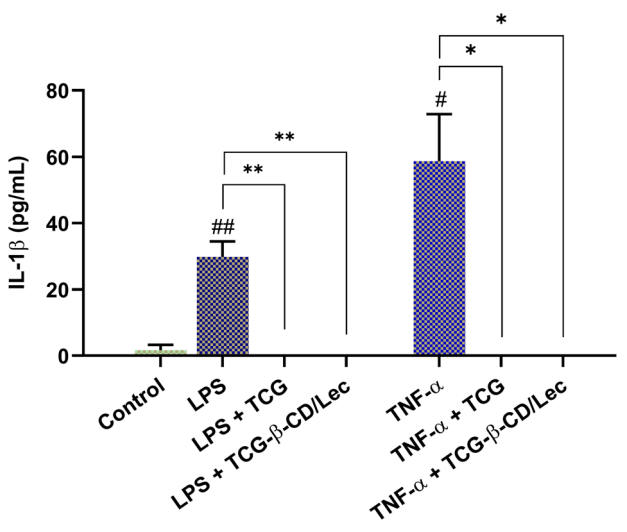

Fig. 11 Effect of TCG and TCG-loaded nano-formulation on IL-1β cytokine production. Graph shows the concentration of IL-1β cytokine in LPS and TNF-α induced SW982 cells treated with TCG and TCG-β-CD/Lec nano-formulation. Data is presented as mean ± SEM ($n = 3$). For multiple comparisons, Tukey's *post hoc* test was applied. Symbol # indicates a significant increase in IL-1β levels compared to the untreated control ($^{\#}p \leq 0.05$, $^{\#\#}p \leq 0.01$). Symbol * indicates a significant reduction in the IL-1β level of the respective groups compared to the LPS or TNF-α control ($^{*}p \leq 0.05$, $^{**}p \leq 0.01$).

IL-1β is a key proinflammatory cytokine implicated in the pathogenesis of RA, primarily secreted by activated monocytes and macrophages in the synovial fluid, contributing to inflammation and joint damage.[59] In line with this, our results demonstrated a marked induction of IL-1β in SW982 cells following LPS and TNF-α stimulation, consistent with previous studies reporting activation of inflammatory cascades and NLRP3 inflammasome signaling by these stimuli.[31,34,60] Treatment with TCG and its nano-formulation significantly attenuated IL-1β levels under both conditions, supporting their potential anti-inflammatory effects. These findings align with earlier reports demonstrating that TCG suppresses IL-1β expression in models of reperfusion injury and diabetic inflammation.[58,61–63] Although these models differ from RA, they underscore TCG's role in modulating IL-1β-mediated inflammatory responses. Collectively, our findings indicate that both TCG and its nano-formulation exert inhibitory effects on inflammatory cytokine production associated with NLRP3 inflammasome activation.

4 Conclusion

The present study utilized SW982 synovial cells to investigate the potential of ticagrelor (TCG) and its nano-formulation in modulating the NLRP3 inflammasome pathway, a known contributor to rheumatoid arthritis (RA) pathogenesis. Both TCG and its nano-formulation demonstrated promising results in suppressing the mRNA expression of NLRP3-related genes, with the ternary complex (TCG-β-CD/Lec) showing superior anti-inflammatory activity and reduced cytotoxicity, suggesting a positive impact of β-CD as a drug delivery carrier. To the best of our knowledge, this may be one of the earliest studies to investigate the role of TCG and its nano-formulation in the context of RA. While the findings are promising, the study is limited to an *in vitro* model and gene expression analysis at the mRNA level. Further studies involving protein-level validation, such as western blotting or immunocytochemistry, are necessary to confirm the observed results. Additionally, *in vivo* studies are essential to evaluate the therapeutic relevance and safety profile of TCG-based formulations in RA. As RA is a multifactorial disease involving various inflammatory pathways beyond NLRP3, future studies should explore the broader immunomodulatory properties of TCG and its nano-formulations across other relevant pathways. Overall, this study provides preliminary evidence supporting the potential therapeutic role of TCG and its β-CD-based nano-formulation in RA and may serve as a basis for further mechanistic and translational research.

Author contributions

Zainab Najam: conceptualization, data curation, formal analysis, funding acquisition, investigation, methodology, software,

visualization, writing – original draft, review and editing. Anum Gul: conceptualization, data curation, formal analysis, funding acquisition, methodology, project administration, resources, supervision, validation, writing – review and editing. Muhammad Kawish: data curation, formal analysis, investigation, visualization, writing – original draft. Muhammad Raza Shah: conceptualization, methodology, resources, supervision. Tooba Aslam: investigation, methodology, software, validation. Nida Dastagir: conceptualization, funding acquisition, methodology, supervision.

Conflicts of interest

The authors declare no potential competing interests.

Data availability

All relevant data supporting the findings of this study are presented in the article.

Acknowledgements

This work was supported by the Sindh Research Support Programme (SRSP) of the Sindh Higher Education Commission (SHEC) (grant number: SHEC/SRSP/Med-5/17/2020- 21) and Vice Chancellors' Seed Funding Initiative (VCSFI) of Dow University of Health Sciences (DUHS) (grant number: DUHS/VC/2023/11-04/31).

References

1 F. A. Figus, M. Piga, I. Azzolin, R. McConnell and A. Iagnocco, *Autoimmun. Rev.*, 2021, **20**, 102776.
2 R. J. Black, M. Cross, L. M. Haile, G. T. Culbreth, J. D. Steinmetz, H. Hagins, J. A. Kopec, P. M. Brooks, A. D. Woolf, K. L. Ong, D. R. Kopansky-Giles, K. E. Dreinhoefer, N. Betteridge, A. Aali, M. Abbasifard, M. Abbasi-Kangevari, A. M. Abdurehman, A. Abedi, H. Abidi, R. G. Aboagye, H. Abolhassani, E. Abu-Gharbieh, A. Abu-Zaid, K. Adamu, I. Y. Addo, M. A. Adesina, Q. E. S. Adnani, M. S. Afzal, A. Ahmed, J. P. Aithala, M. Akhlaghdoust, A. Alemayehu, S. Alvand, N. J. Alvis-Zakzuk, H. Amu, B. Antony, J. Arabloo, A. Y. Aravkin, J. Arulappan, T. Ashraf, S. S. Athari, S. Azadnajafabad, A. Badawi, N. Baghcheghi, A. A. Baig, A. B. Balta, M. Banach, P. C. Banik, A. Barrow, A. Bashiri, L. M. Bearne, A. Bekele, I. M. Bensenor, A. Y. Berhie, A. S. Bhagavathula, P. Bhardwaj, A. N. Bhat, V. S. Bhojaraja, S. Bitaraf, B. B. A. Bodicha, J. S. Botelho, A. M. Briggs, R. Buchbinder, C. A. Castañeda-Orjuela, P. Charalampous, V. K. Chattu, K. Coberly, N. Cruz-Martins, O. Dadras, X. Dai, K. de Luca, F. N. Dessalegn, G. Dessie, M. Dhimal, L. E. Digesa, M. Diress, P. N. Doku, H. A. Edinur, M. Ekholuenetale, M. Elhadi, Y. M. El-Sherbiny, F. Etaee, R. Ezzeddini, S. Faghani, I. Filip, F. Fischer, T. Fukumoto, B. Ganesan, M. A. Gebremichael, U. Gerema, M. E. Getachew, A. Ghashghaee, T. K. Gill, B. Gupta, S. Gupta, V. B. Gupta, V. K. Gupta, R. Halwani, M. A. Hannan, S. Haque, N. I. Harlianto, M. Harorani, A. I. Hasaballah, M. B. Hassen, S. I. Hay, K. Hayat, G. Heidari, K. Hezam, C. L. Hill, Y. Hiraike, N. Horita, A. H. Hoveidaei, A. K. Hsiao, E. Hsieh, S. Hussain, I. Iavicoli, I. M. Ilic, S. M. S. Islam, N. E. Ismail, M. Iwagami, M. Jakovljevic, C. T. Jani, J. Jeganathan, N. Joseph, V. Kadashetti, H. Kandel, T. K. Kanko, I. M. Karaye, H. Khajuria, M. J. Khan, M. A. B. Khan, J. Khanali, M. M. Khatatbeh, J. Khubchandani, Y. J. Kim, A. Kisa, A.-A. Kolahi, F. Kompani, H. R. Koohestani, A. Koyanagi, K. Krishan, M. Kuddus, N. Kumar, A. Kuttikkattu, B. Larijani, S. S. Lim, J. Lo, V. S. Machado, P. B. Mahajan, A. Majeed, E. M. Rad, A. A. Malik, M. A. Mansournia, E. Mathews, J. J. Mendes, A.-F. A. Mentis, M. K. Mesregah, T. Mestrovic, S. P. Mirghaderi, E. M. Mirrakhimov, A. Misganaw, A. Mohamadkhani, S. Mohammed, A. H. Mokdad, M. Moniruzzaman, A. A. Montasir, G. B. Mulu, E. Murillo-Zamora, C. J. L. Murray, G. Mustafa, M. Naghavi, T. S. Nair, A. A. Naqvi, Z. S. Natto, B. P. Nayak, S. Neupane, C. T. Nguyen, R. K. Niazi, O. J. Nzoputam, I.-H. Oh, H. Okati-Aliabad, O. C. Okonji, I. I. Olufadewa, M. O. Owolabi, K. Pacheco-Barrios, J. R. Padubidri, J. Patel, A. R. Pathan, S. Pawar, P. Pedersini, A. Perianayagam, I.-R. Petcu, I. Qattea, A. Radfar, A. Rafiei, M. H. U. Rahman, V. Rahmanian, V. Rashedi, M.-M. Rashidi, Z. A. Ratan, S. Rawaf, M. S. Razeghinia, E. M. M. Redwan, A. M. N. Renzaho, N. Rezaei, N. Rezaei, A. Riad, A. M. A. Saad, B. Saddik, U. Saeed, A. Safary, M. Sahebazzamani, A. Sahebkar, H. Sahoo, A. Salek Farrokhi, M. A. N. Saqib, A. Seylani, S. Shahabi, M. A. Shaikh, B. B. Shashamo, A. Shetty, J. K. Shetty, M. Shigematsu, V. Shivarov, P. Shobeiri, M. M. Sibhat, E. Sinaei, A. Singh, J. A. Singh, P. Singh, S. Singh, M. S. Siraj, A. A. Skryabina, H. Slater, A. E. Smith, Y. Solomon, M. S. Soltani-Zangbar, M. Tabish, K.-K. Tan, N. Y. Tat, A. Tehrani-Banihashemi, S. Tharwat, M. R. Tovani-Palone, B. S. Tusa, S. V. Tahbaz, P. R. Valdez, R. Valizadeh, S. Vaziri, S. E. Vollset, A.-M. Wu, D. Y. Yada, S. S. Yehualashet, N. Yonemoto, Y. You, I. Yunusa, M. Zangiabadian, I. Zare, A. Zarrintan, Z.-J. Zhang, C. Zhong, M. Zoladl, T. Vos and L. M. March, *Lancet Rheumatol.*, 2023, **5**, e594–e610.
3 V. C. Romão and J. E. Fonseca, *Front. Med.*, 2021, **8**, 689698.
4 V. L. Kronzer and J. M. r. Davis, *Curr. Rheumatol. Rep.*, 2021, **23**, 21.
5 Q. Fang, C. Zhou and K. S. Nandakumar, *Mediators Inflammation*, 2020, **2020**, 3830212.
6 M. F. Bustamante, R. Garcia-Carbonell, K. D. Whisenant and M. Guma, *Arthritis Res. Ther.*, 2017, **19**, 110.
7 J. Huang, X. Fu, X. Chen, Z. Li, Y. Huang and C. Liang, *Front. Immunol.*, 2021, **12**, 686155.
8 L. Spel and F. Martinon, *Immunol. Rev.*, 2020, **294**, 48–62.
9 K. V. Swanson, M. Deng and J. P. Y. Ting, *Nat. Rev. Immunol.*, 2019, **19**, 477–489.

10 H.-H. Shen, Y.-X. Yang, X. Meng, X.-Y. Luo, X.-M. Li, Z.-W. Shuai, D.-Q. Ye and H.-F. Pan, *Autoimmun. Rev.*, 2018, **17**, 694–702.
11 X. Chen, P. Zhang, Y. Zhang, M. Wei, T. Tian, D. Zhu, Y. Guan, W. Wei and Y. Ma, *Cell. Immunol.*, 2024, **397–398**, 104810.
12 B. Springthorpe, A. Bailey, P. Barton, T. N. Birkinshaw, R. V. Bonnert, R. C. Brown, D. Chapman, J. Dixon, S. D. Guile, R. G. Humphries, S. F. Hunt, F. Ince, A. H. Ingall, I. P. Kirk, P. D. Leeson, P. Leff, R. J. Lewis, B. P. Martin, D. F. McGinnity, M. P. Mortimore, S. W. Paine, G. Pairaudeau, A. Patel, A. J. Rigby, R. J. Riley, B. J. Teobald, W. Tomlinson, P. J. H. Webborn and P. A. Willis, *Bioorg. Med. Chem. Lett.*, 2007, **17**, 6013–6018.
13 G. J. J. Van, L. Nilsson, P. Berntsson, B. M. Wissing, F. Giordanetto, W. Tomlinson and P. J. Greasley, *J. Thromb. Haemostasis*, 2009, **7**, 1556–1565.
14 G. C. Herron and E. R. Bates, *J. Am. Heart Assoc.*, 2024, **13**, e031606.
15 B. Huang, Y. Qian, S. Xie, X. Ye, H. Chen, Z. Chen, L. Zhang, J. Xu, H. Hu, S. Ma, P. Héroux, D. Wang, H.-M. Shen, Y. Wu and D. Xia, *Cell. Mol. Immunol.*, 2021, **18**, 1278–1289.
16 H. Chen, D. Tran, H.-C. Yang, S. Nylander, Y. Birnbaum and Y. Ye, *Cardiovasc. Drugs Ther.*, 2020, **34**, 443–461.
17 Y. Birnbaum, H. Chen, D. Tran, S. Nylander and Y. Ye, *Cardiovasc. Drugs Ther.*, 2022, **36**, 829–840.
18 F. Li, D. Xu, K. Hou, X. Gou, N. Lv, W. Fang and Y. Li, *J. Neuroimmune Pharmacol.*, 2021, **16**, 835–853.
19 S.-h. Wang, M.-j. Sun, S.-y. Ding, C.-l. Liu, J.-m. Wang, S.-n. Han, X. Lin and Q. Li, *Front. Cardiovasc. Med.*, 2023, **9**, 1090601.
20 Y. Birnbaum, G. D. Birnbaum, I. Birnbaum, S. Nylander and Y. Ye, *Cardiovasc. Drugs Ther.*, 2016, **30**, 539–550.
21 *Chemistry Review(s), Report 022433Orig1s000 Center for Drug Evaluation and Research*, FDA, 2011.
22 C. M. Hosey, R. Chan and L. Z. Benet, *AAPS J.*, 2016, **18**, 251–260.
23 R. Teng and J. Maya, *J. Drug Assess.*, 2014, **3**, 43–50.
24 Á. Sarabia-Vallejo, M. D. M. Caja, A. I. Olives, M. A. Martín and J. C. Menéndez, *Pharmaceutics*, 2023, **15**(9), 2345.
25 G. Crini, S. Fourmentin, É. Fenyvesi, G. Torri, M. Fourmentin and N. Morin-Crini, *Environ. Chem. Lett.*, 2018, **16**, 1361–1375.
26 G. Tiwari, R. Tiwari and A. K. Rai, *J. Pharm. BioAllied Sci.*, 2010, **2**, 72–79.
27 S. V. Kurkov and T. Loftsson, *Int. J. Pharm.*, 2013, **453**, 167–180.
28 I. Puskás, L. Szente, L. Szőcs and É. Fenyvesi, *Period. Polytech., Chem. Eng.*, 2023, **67**(1), 11–17.
29 N. Fatima, S. H. Khalid, K. Liaqat, A. Zulfiqar and R. Munir, *Polym. Sci.*, 2023, **4**(5), 000597.
30 J. H. Chang, K. J. Lee, S. K. Kim, D. H. Yoo and T. Y. Kang, *Indian J. Med. Res.*, 2014, **139**, 117–124.
31 M. Khansai, T. Phitak, J. Klangjorhor, S. Udomrak, K. Fanhchaksai, P. Pothacharoen and P. Kongtawelert, *BMC Complementary Altern. Med.*, 2017, **17**, 532.
32 K. Więcek, P. Kupczyk, G. Chodaczek and M. Woźniak, *J. Immunol. Res.*, 2022, **2022**, 1208970.
33 B. Rakhecha, P. Agnihotri, T. C. Dakal, M. Saquib, Monu and S. Biswas, *Biosci. Rep.*, 2022, **42**(4), BSR20211392.
34 Y. Zhao, Y. Chen, J. Wang, X. Zhu, K. Wang, Y. Li and F. Zhou, *Mol. Med. Rep.*, 2021, **24**(2), 555.
35 H. E. Pence and A. Williams, *J. Chem. Educ.*, 2010, **87**, 1123–1124.
36 R. Siddiqui, A. Boghossian, S. S. Alqassim, M. Kawish, J. Gul, T. Jabri, M. R. Shah and N. A. Khan, *Arch. Microbiol.*, 2023, **205**, 170.
37 J. van Meerloo, G. J. L. Kaspers and J. Cloos, in *Cancer Cell Culture: Methods and Protocols*, ed. I. A. Cree, Humana Press, Totowa, NJ, 2011, pp. 237–245, DOI: **10.1007/978-1-61779-080-5_20**.
38 H. Kim and X. Xue, *J. Vis. Exp.*, 2020, **160**, e60682.
39 C. A. Schneider, W. S. Rasband and K. W. Eliceiri, *Nat. Methods*, 2012, **9**, 671–675.
40 J. Ye, G. Coulouris, I. Zaretskaya, I. Cutcutache, S. Rozen and T. L. Madden, *BMC Bioinf.*, 2012, **13**, 134.
41 W. A. Kibbe, *Nucleic Acids Res.*, 2007, **35**, W43–W46.
42 F. Zhou, L. Yu, Y. Liu, Z. Zeng, C. Li, Z. Fang, B. Hu, H. Chen, C. Wang, S. Chen, H. Wu, W. Wu and Y. Liu, *Int. J. Biol. Macromol.*, 2023, **235**, 123802.
43 S. Waheed, Z. Li, F. Zhang, A. Chiarini, U. Armato and J. Wu, *J. Nanobiotechnol.*, 2022, **20**, 395.
44 I. Javed, S. Z. Hussain, I. Ullah, I. Khan, M. Ateeq, G. Shahnaz, H. ur Rehman, M. T. Razi, M. R. Shah and I. Hussain, *J. Mater. Chem. B*, 2015, **3**, 8359–8365.
45 N. Shahid, A. Erum, M. Zaman, U. R. Tulain, Q.-U.-A. Shoaib, A. Majeed, M. F. Rasool, I. Imran, S. Alshehri, B. Noorani and F. Alqahtani, *Int. J. Nanomed.*, 2021, **16**, 6345–6366.
46 A. A. A. Alsaad, *J. ReAtt. Ther. Dev. Divers*, 2022, **5**, 494–505.
47 X. Wang, Z. Luo and Z. Xiao, *Carbohydr. Polym.*, 2014, **101**, 1027–1032.
48 M. Imran, M. R. Shah, F. Ullah, S. Ullah, A. M. A. Elhissi, W. Nawaz, F. Ahmad, A. Sadiq and I. Ali, *Int. J. Pharm.*, 2016, **505**, 122–132.
49 T. Jabri, M. Imran, Shafiullah, K. Rao, I. Ali, M. Arfan and M. R. Shah, *Carbohydr. Polym.*, 2018, **194**, 89–96.
50 S. Hong, D. W. Choi, H. N. Kim, C. G. Park, W. Lee and H. H. Park, *Pharmaceutics*, 2020, **12**(7), 604.
51 *Biological Evaluation of Medical Devices—Part 5: Tests for In vitro Cytotoxicity, Report ISO 10993-5:2009*, International Organization for Standardization, Switzerland, 2009.
52 G.-H. Son, Y.-G. Na, H. W. Huh, M. Wang, M.-K. Kim, M.-G. Han, J.-J. Byeon, H.-K. Lee and C.-W. Cho, *Pharmaceutics*, 2019, **11**(5), 222.
53 S.-J. Kim, H.-K. Lee, Y.-G. Na, K.-H. Bang, H.-J. Lee, M. Wang, H.-W. Huh and C.-W. Cho, *Int. J. Pharm.*, 2019, **555**, 11–18.
54 Y.-G. Na, J.-J. Byeon, M. Wang, H. W. Huh, G.-H. Son, S.-H. Jeon, K.-H. Bang, S.-J. Kim, H.-J. Lee, H.-K. Lee and C.-W. Cho, *Int. J. Nanomed.*, 2019, **14**, 1193–1212.
55 X. Wang, X. Han, M. Li, Y. Han, Y. Zhang, S. Zhao and Y. Li, *Microvasc. Res.*, 2018, **119**, 98–104.
56 Y. Olgar, E. Tuncay, D. Billur, A. Durak, S. Ozdemir and B. Turan, *Mol. Cell. Biochem.*, 2020, **469**, 97–107.

57 C. V. Bitirim, Z. B. Ozer, D. Aydos, K. Genc, S. Demirsoy, K. C. Akcali and B. Turan, *Sci. Rep.*, 2022, **12**, 5651.
58 X. Xu, H. Zhang, L. Li, R. Yang, G. Li, S. Liu, G. Schmalzing, H. Nie and S. Liang, *Mol. Neurobiol.*, 2022, **59**, 1604–1618.
59 K. Wang, H. Luo, L. Liu, H. Gao, Y. Song and D. Li, *Front. Pharmacol*, 2025, **16**, 1577628.
60 C. Choulaki, G. Papadaki, A. Repa, E. Kampouraki, K. Kambas, K. Ritis, G. Bertsias, D. T. Boumpas and P. Sidiropoulos, *Arthritis Res. Ther.*, 2015, **17**, 257.
61 Y.-h. Cao, Q.-c. Xu, Y.-w. Wang, Y. Ling and C. Fu, *Curr. Med. Sci.*, 2022, **42**, 505–512.
62 C. Yu, C.-M. Gao, N. Xie, X.-Q. Wang and Y.-Q. Ma, *Exp. Ther. Med.*, 2021, **21**, 475.
63 X. Li, Y. Li, K. Shen, H. Li and J. Bai, *Platelets*, 2019, **30**, 199–205.